Compact, Watt-class 785 nm dual-wavelength master oscillator power amplifiers

Journal of Physics Communications

PAPER

Compact, Watt-class 785 nm dual-wavelength master oscillator power amplifiers

André Müller, Martin Maiwald and Bernd Sumpf

Ferdinand Braun Institut (FBH), Gustav-Kirchhoff-Str. 4, 12489 Berlin, Germany

E-mail: andre.mueller@fbh-berlin.de

Keywords: master oscillator power amplifier, diode laser, distributed Bragg reflector, tapered amplifier, dual-wavelength, Raman spectroscopy

OPEN ACCESS

RECEIVED
12 September 2022

REVISED
8 November 2022

ACCEPTED FOR PUBLICATION
16 December 2022

PUBLISHED
27 December 2022

Abstract

785 nm micro-integrated, dual-wavelength master oscillator power amplifiers with a footprint of 5 mm × 25 mm are presented. They are based on Y-branch distributed Bragg reflector ridge waveguide diode lasers and anti-reflection coated tapered amplifiers. In order to reduce the impact of potential optical feedback, devices with master oscillator front facet reflectivities of 5% and 30% as well as with an integrated miniaturized optical isolator have been realized. A comparison up to 1 W shows narrowband dual wavelength laser emission with a spectral distance of 0.6 nm (10 cm^{-1}) and individual spectral widths <20 pm. As expected, a higher front facet reflectivity leads to a significant reduction of feedback related mode hops. Longitudinal modes corresponding to the master oscillator resonator length remain within spectral windows <0.15 nm (3 cm^{-1}), suitable for applications such as Raman spectroscopy and especially shifted excitation Raman difference spectroscopy. Integrating a compact 30 dB optical isolator completely eliminates the observed optical feedback effects. Lateral beam propagation ratios of 1.2 ($1/e^2$) enable easy beam shaping and fiber coupling. Outside of the experimental comparison, the developed MOPAs provide up to 2.7 W of optical output power available for applications.

1. Introduction

Background disturbances pose a significant challenge for *in situ* Raman measurements and Raman spectroscopy outside of traditional laboratory environments. Signal contributions by fluorescence can mask weaker Raman signals due to the much lower Raman scattering cross section [1, 2]. To extract Raman signals under these conditions, methods such as time-gated Raman spectroscopy [3, 4] and Fourier-transform Raman spectroscopy [1] as well as target excitation in the deep-UV spectral range [5, 6] have been demonstrated. For spectral separation between Raman signals and background disturbances such as ambient daylight or fixed pattern noise, techniques based on shifted excitation wavelengths have been presented [7–14]. The spectral position of the observed Raman signal follows the excitation wavelength change, while non-Raman signals remain spectrally constant.

In case of shifted excitation Raman difference spectroscopy (SERDS), only two excitation wavelengths are required and Raman spectra are obtained by subtraction of two recorded spectra [15]. Excitation light sources suitable for SERDS should provide alternating dual-wavelength laser emission. In order to resolve Raman signal bandwidths of most solid and liquid samples, the spectral widths at both wavelengths and their spectral distance should be within 3 cm^{-1} to 10 cm^{-1}. High spatial beam qualities allow for easy beam shaping and fiber coupling, required for fiber-based probes. In order to realize portable laser systems, the light sources should also be compact with a low power consumption and without movable parts.

At 785 nm, a wavelength well-established for Raman spectroscopy, monolithic dual-wavelength Y-branch distributed Bragg reflector (DBR) ridge waveguide (RW) diode lasers with 200 mW optical output power, a beam propagation ratio of $M^2 < 2$ ($1/e^2$) and a lifetime tested up to 3,800 h have been presented [16]. Their

compact size and low power consumption enabled the realization of portable laser systems for SERDS and their *in situ* application in field experiments outside the lab [17].

Low concentrations, short measurement times, weak Raman scatterers, or measurements at a distance in a stand-off arrangement may require Watt-class excitation powers [1, 18]. The latter can be obtained in a master oscillator power amplifier (MOPA) configuration [19] that, unlike monolithic wavelength stabilized high-power diode lasers, also enables nearly constant excitation wavelengths along the entire power range. A micro-integrated dual-wavelength MOPA with a Y-branch DBR laser and a tilted RW amplifier on a 5 mm × 25 mm micro optical bench provided 0.5 W at 785 nm [20]. Such MOPAs provide stable excitation wavelengths and therefore enable a flexibility in output powers without requiring spectral recalibrations of applied spectrometers. The MOPA also eliminated the spatial tilt between far field intensity distributions at both wavelengths, which can be critical for fiber coupling and has been observed for Y-branch DBR diode lasers [16]. To exceed the optical output power available with a RW amplifier while maintaining the spatial beam quality, 785 nm tapered power amplifiers could be used [21].

In this work, compact, Watt-class dual-wavelength MOPAs at 785 nm based on Y-branch DBR RW lasers and tapered amplifiers on 5 mm × 25 mm micro optical benches are presented. A challenge for micro-integrated MOPA configurations is the suppression or elimination of optical feedback from the amplifier into the master oscillator that otherwise may affect the spectral characteristics required for the application [22, 23]. For comparison, two MOPAs with master oscillator front facet reflectivities of 5% and 30% and a MOPA with an implemented miniaturized 30 dB optical isolator are realized.

2. Layer structures and lateral designs

All master oscillators (MO) and power amplifiers (PA) evaluated in this work are grown with metal organic vapor phase epitaxy. As MOs, 785 nm Y-branch DBR lasers based on a GaAsP single quantum well symmetrically embedded in a 1 μm AlGaAs waveguide are used [24]. The corresponding vertical far field angles are 26° at full width at half maximum (FWHM) and 48° measured at $1/e^2$ (figure 1).

Processed 3 mm long devices consist of two coupled DBR RW laser cavities (figure 2). The passive, 500 μm long, 10th order gratings (DBR_1, DBR_2) are separated laterally by 80 μm. They serve as wavelength selective rear side cavity mirrors and are individually designed for dual-wavelength operation with an intended spectral distance of 0.6 nm (10 cm^{-1}) between the laser emission wavelengths. Considering commercially available Raman filters, the grating periods have been processed for wavelength-stabilized laser emissions at target wavelength regions of 784 nm and 785 nm.

Laser emission within the device is index guided via 2.2 μm wide RWs. An S-bend shaped Y-branch with a length of 2 mm is realized to couple emission from the single waveguides into a common 500 μm long output waveguide. For operation, the electric contacts are divided in four sections and enable alternating dual-wavelength laser emission. These include 1.35 mm long contacts for the two branches (I_1, I_2), a 0.20 mm long contact for the Y-branch coupling section (I_Y), and a 0.95 mm long contact for the common output (I_{Out}). Both laser facets are passivated [25] and anti-reflection (AR) coated with 5% and 30% on the front facet and $< \times 10^{-3}$ on the rear facet, respectively.

As PAs, 785 nm tapered amplifiers based on a GaAsP single quantum well symmetrically embedded in a 2 μm AlGaAs waveguide have been developed. The measured vertical far field angles are 24° (FWHM) and 40° ($1/e^2$), respectively. All amplifiers consist of a 2 mm long RW with a waveguide width of 3 μm and a 2 mm long tapered section with a full angle of 6° (figure 2). Each section can be operated individually (I_{RW}, I_{TA}). All amplifier facets are passivated and AR coated with a measured reflectivities $<1 \times 10^{-3}$.

3. Concepts for compact dual-wavelength MOPAs

Based on the above devices, three MOPA configurations are realized (figure 3). In all concepts, MO and PA are soldered p-side up on copper tungsten (CuW) heat spreaders on 5 mm × 25 mm aluminum nitride (AlN) micro optical benches using AuSn. This solder has been previously evaluated for mounting of high-power laser diodes [26]. The subassemblies are mounted on conduction cooled package mounts with footprints of 25 mm × 25 mm using PbSn.

Collimation and coupling of laser emission are obtained with micro cylindrical lenses (Ingeneric GmbH), AR coated for 785 nm with R < 1%. For beam shaping in vertical direction, fast axis collimation lenses (FAC) with a focal length of f = 0.6 mm, a numerical aperture of NA = 0.8 and dimensions of L × W × H = 0.8 mm × 1.5 mm × 1.0 mm are used. Lateral beam shaping is obtained with slow axis collimation lenses (SAC) with f = 2.3 mm, NA = 0.3, and edge lengths of 1.5 mm. All optics are positioned with a six-axis alignment stage (SmarAct GmbH) and mounted using an UV-light curable adhesive.

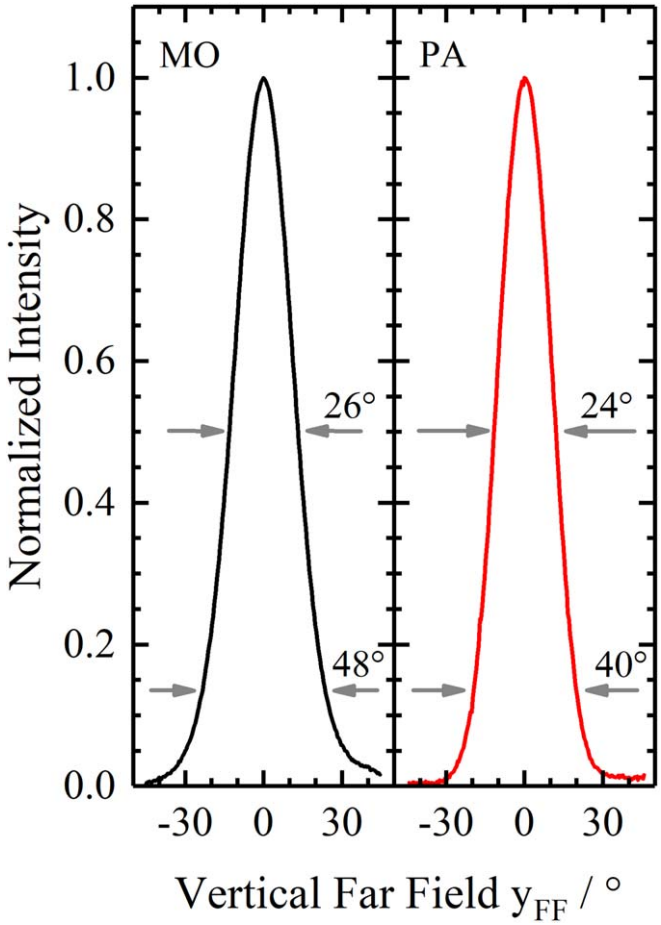

Figure 1. Vertical far field intensity distributions of layer structures applied for Y-branch DBR lasers (MO) and tapered amplifiers (PA).

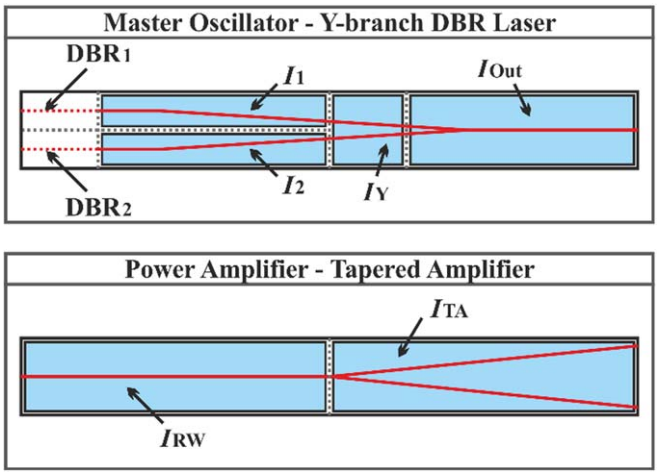

Figure 2. Illustrations of the lateral layouts for master oscillators and power amplifiers in this study.

The MOPAs in concept 1 and 2 differ from one another only in the front facet reflectivity of the MOs ($R_{F,MO}$). Here, a Y-branch DBR laser with 5% is selected for concept 1 while a laser with 30% is used in concept 2.

In concept 3, a MOPA with a 5% AR coated MO and a miniaturized, cylindrical 30 dB optical isolator (Isowave) between MO and PA is realized. The 5 mm long isolator has a clear aperture of 1.4 mm at an outer diameter of 4.0 mm. Its specified maximum insertion loss is $\leqslant$4 dB. In order to adapt the beam height with respect to the isolator while avoiding changes to the micro optical bench or the conduction cooled package mount, MO and PA are mounted on three CuW heat spreaders. The round isolator is manually positioned in

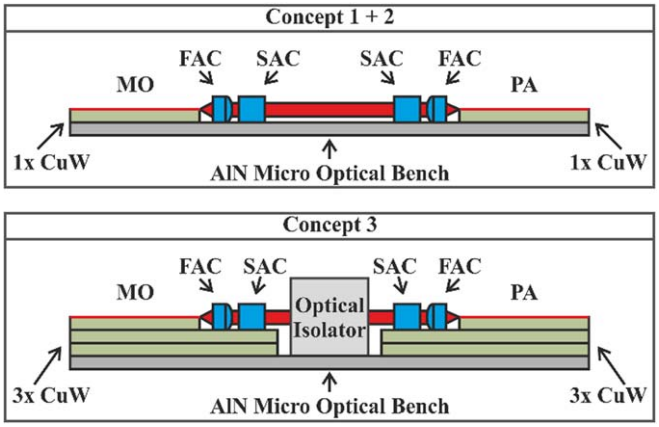

Figure 3. Illustrations of the optical concepts for dual-wavelength MOPAs compared in this study.

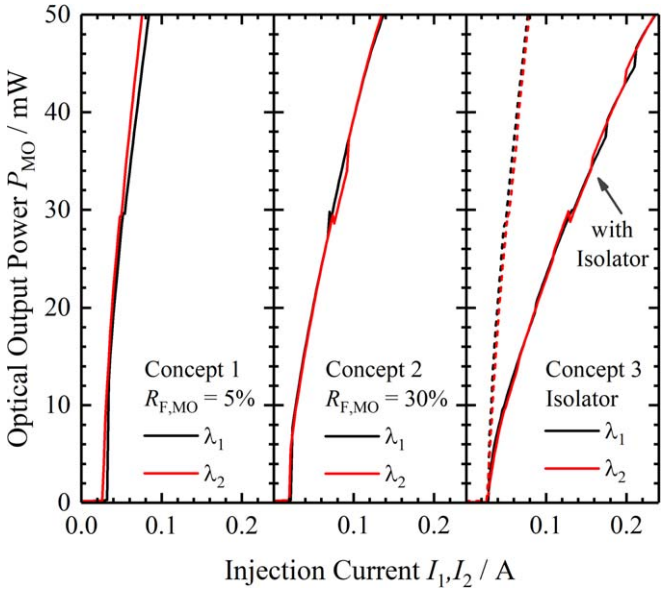

Figure 4. Master oscillator power-current characteristics at 25 °C.

between AlN supports, which have been glued to the micro optical bench in advance, and mounted with the previously mentioned UV-light curable adhesive.

4. Dual-wavelength master oscillators

For all measurements, the MOPAs are individually mounted on a Peltier-cooled heat sink that is set to a temperature of $T = 25$ °C. Similar to previous reports [12], the MOs are operated in continuous wave (CW) operation with $I_{Out} = 35$ mA and the Y-branch section not connected. Figure 4 shows the power-current characteristics of the MOs up to 50 mW. The latter was previosly determined as amplifier seed power in saturation measurements. With the PAs already soldered onto the micro optical benches, the collimated laser emissions have been redirected to a power detector using a high-reflection coated prism. The injection currents to the branches of the MOs (I_1, I_2) are applied individually and increased in 2 mA steps.

For each Y-branch laser, comparable power-current characteristics are obtained at both wavelengths. All curves show a rapid increase to about 10 mW around threshold, followed by a linear progression of output power as a function of the injection currents. In case of the 5% AR coated MO in concept 1, laser emission is obtained at about 30 mA and 50 mW are measured at 80 mA. The slope efficiency measured between 25 mW and 50 mW is 0.65 W A^{-1}.

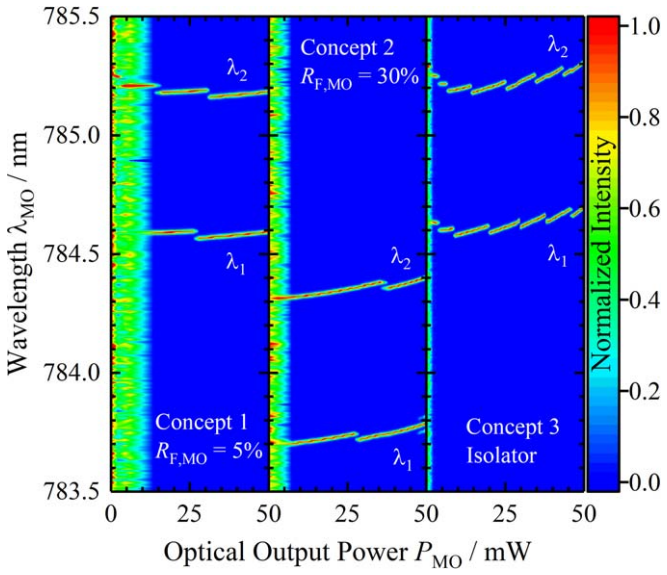

Figure 5. Master oscillator spectral characteristics at 25 °C.

As expected, the 30% facet reflectivity for the MO in concept 2 reduces the lasing threshold and slope efficiency to about 20 mA and 0.33 W A^{-1}, respectively. Output powers of 50 mW are therefore obtained at 140 mA.

As also expected, power-current characteristics of the 5% AR coated MO in concept 3 are similar to the laser in concept 1. However, the specified insertion loss of $\leqslant$4 dB reduces the obtained output power from 50 mW at 80 mA to about 18 mW after propagation through the isolator. As a result, 50 mW are measured at about 240 mA. The corresponding power consumption including the operation of the common output is about 0.6 W.

A comparison of the corresponding spectral characteristics is presented in figure 5. All spectra are measured with a double Echelle monochromator with a spectral resolution of 10 pm at 785 nm (LTB Lasertechnik Berlin GmbH). Each spectrum is individually normalized in intensity to 1 and both wavelengths versus optical output power are shown combined in the plots.

All MOs provide narrowband dual-wavelength laser emissions and temperature related mode hops, typical for DBR lasers. The spectral distance covered by the mode hops is about 30 pm and fits to the free spectral range for 3.0 mm long laser resonators. Due to the increased injection current required for 50 mW, a higher number of mode hops is observed for the Y-branch laser in concept 3. Not shown in this plot, the temperature related wavelength shifts in between mode hops are about 1 pm mA^{-1} (0.02 cm^{-1} mA^{-1}). In all cases, a spectral distance of about 0.6 nm (10 cm^{-1}) is measured between both laser emission wavelengths.

At threshold, the 5% AR coated MO in concept 1 shows laser emissions at 784.59 nm and 785.21 nm. The lower threshold for λ_2 correlates with the electro-optical characteristics in figure 4. At 50 mW, laser emission wavelengths of 784.60 nm and 758.18 nm are measured.

The 30% AR coated MO in concept 2, with gratings designed for the second target wavelength region, provides laser emissions at 783.70 nm and 784.32 nm. Due to the higher front facet reflectivity and its effect on the slope efficiency, both laser emission wavelengths slightly shift towards longer wavelengths at higher output powers. At 50 mW, emission wavelengths of 783.77 nm and 784.40 nm are measured.

Compared to the MO in concept 1, the 5% AR coated MO in concept 3 with additional submounts provides slightly longer emission wavelengths at threshold. Here, peak wavelengths of about 784.63 nm and 785.25 nm are measured. Again, temperature related wavelength shifts can be observed and emission wavelengths of 784.70 nm and 785.28 nm are obtained at 50 mW.

The corresponding single emission spectra at 50 mW are provided in figure 6. The plot shows single mode spectra at both wavelengths with spectral widths of 20 pm (FWHM) for all three lasers. The latter are limited by the spectral resolution of the spectrum analyzer.

5. Master oscillator power amplifiers

Based on the optical concepts illustrated in figure 3, laser emissions of the Y-branch DBR lasers with the previously discussed electro-optical and spectral characteristics are coupled into tapered amplifiers for MOPA configurations. As an example, the resulting MOPA configurations are characterized with $I_{RW} = 200$ mA.

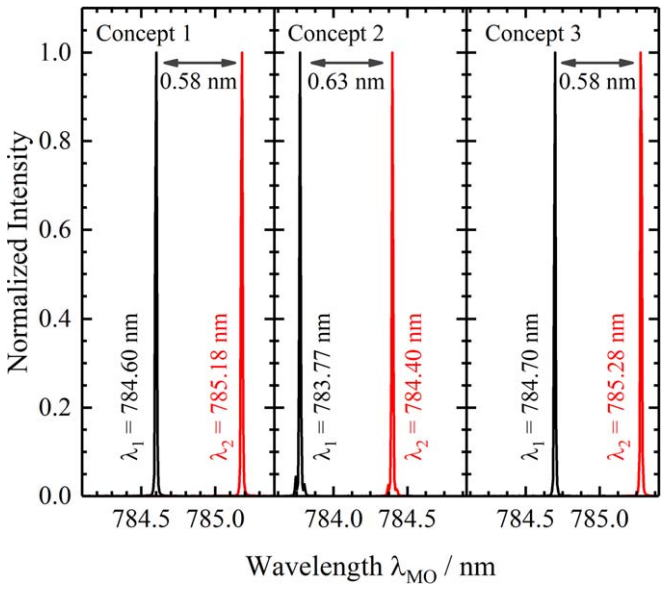

Figure 6. Master oscillator emission spectra at 50 mW.

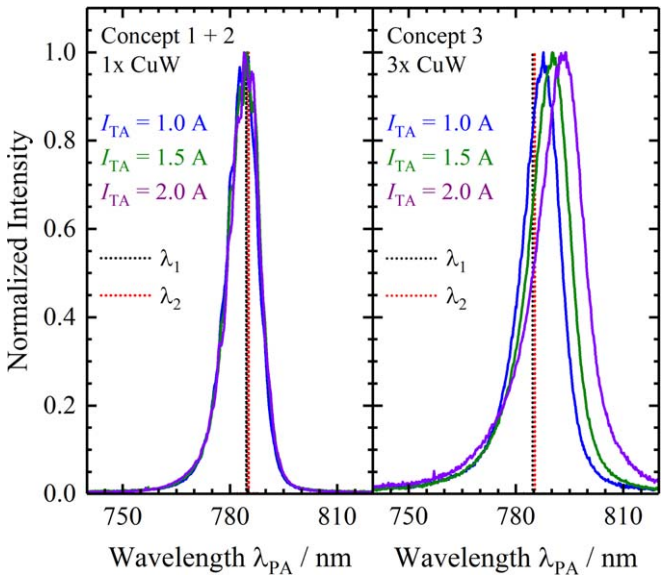

Figure 7. Normalized spontaneous emission spectra for power amplifiers in configurations with different numbers of CuW heat spreaders. Dotted lines represent normalized emission spectra of the MOs at 50 mW.

As described above, the MOPA in concept 3 is realized with a higher number of CuW heat spreaders compared to the concepts 1 and 2. Figure 7 shows the resulting spontaneous emission spectra for amplifiers in both configurations with respect to the emission wavelengths for the 5% AR coated MOs at 50 mW. In case of the configuration with a single CuW heat spreader, the spontaneous emission spectra of the amplifier remain comparable at all settings and overlap with the MO emission wavelengths. In the other case with three heat spreaders, a shift of the amplifier emission spectra is observed and indicates a reduced conduction of heat. At 1 A, the spectral position is red-shifted by about 3 nm with respect to the MO emission wavelengths. That mismatch increases to about 9 nm at 2 A and could affect the corresponding power amplification.

Figure 8 shows the obtained power-current characteristics for all MOPAs up to a target power of 1 W selected for comparison. The injection currents to the tapered sections are increased in 20 mA steps.

As expected, a common seed power results in a comparable performance of the MOPAs without an optical isolator. An output power of 1 W is obtained at about 1.30 A in concept 1 and 1.36 A in concept 2. The measured

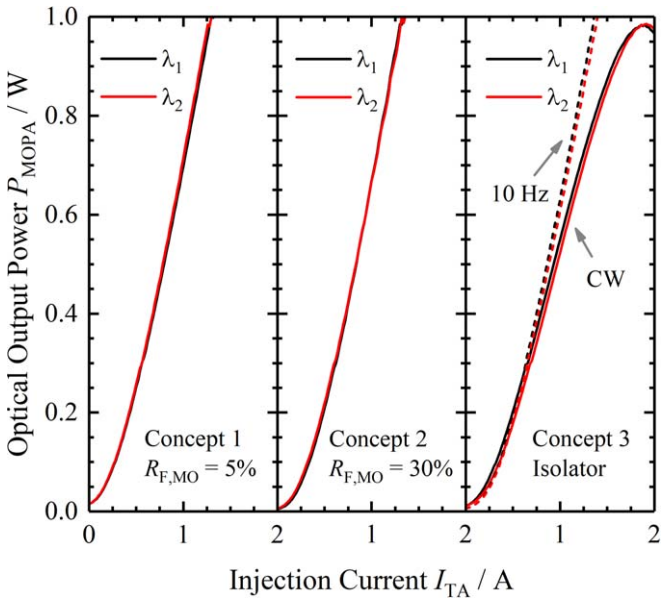

Figure 8. Power-current characteristics for MOPAs at 50 mW pump power. Dashed lines indicate modulated amplifier operation.

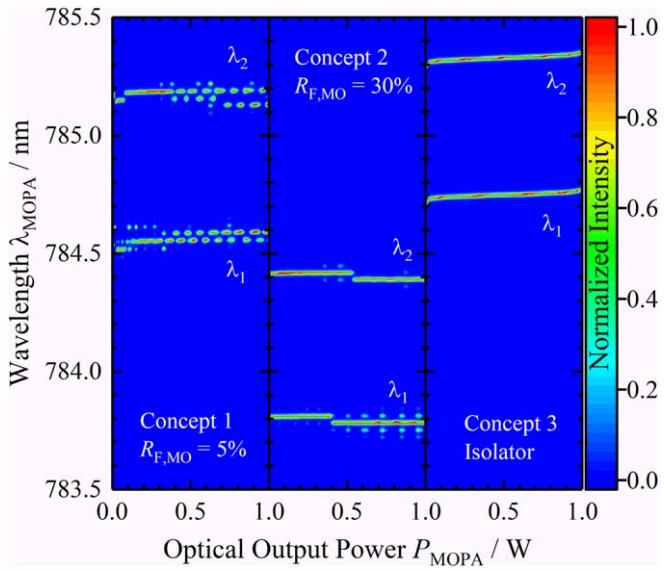

Figure 9. Spectral characteristics for MOPAs at 50 mW pump power.

slope efficiencies are 0.76 W A^{-1} and 0.74 W A^{-1}, respectively. For both devices, power consumptions of 2.9 W in concept 1 and 3.1 W in concept 2 are measured, including the operation of the RWs and MOs.

For the MOPA with the optical isolator, a roll-over at injection currents of about 1.9 A limits the obtained optical output powers to 0.98 W. The corresponding power consumption is about 4.6 W. In order to confirm that the observed roll-over is temperature related, the injection current to the tapered section is modulated at a frequency of 10 Hz and a duty cycle of 50%. The laser emission is detected using a photodiode and converted into optical output power. In these measurements, a peak output power of 1 W at about 1.4 A and a slope efficiency of 0.71 W A^{-1} are obtained. The results are comparable to the MOPAs in the other two configurations due to the common seed power in conjunction with less heat generated under modulated operation of the amplifier.

Figure 9 provides a comparison of the spectral characteristics in CW operation. Each spectrum is individually normalized in intensity to 1 and both wavelengths versus optical output power are combined in the plots.

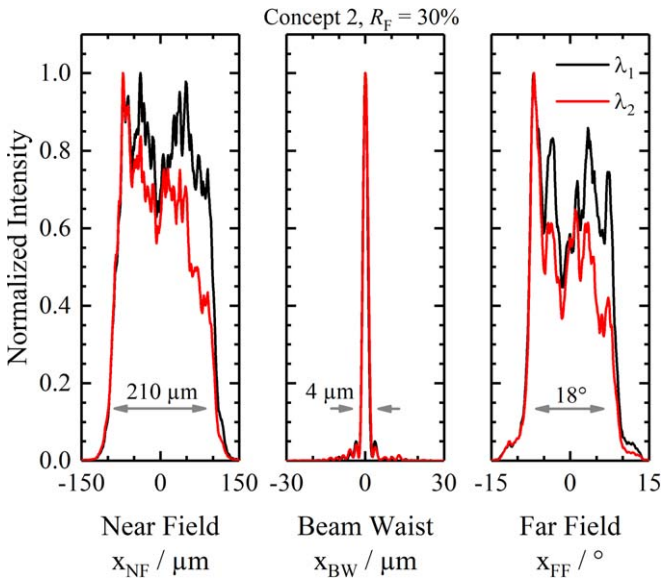

Figure 10. Lateral intensity distributions of near fields, beam waists and far fields for the concept 2 MOPA at 1 W.

All measurements show stable narrowband emission over the entire power range. However, random mode hops and simultaneous longitudinal modes are observed. They remain within spectral windows <0.15 nm (3 cm^{-1}) at both wavelengths, suitable for Raman spectroscopy and SERDS. A spectral distance of about 30 pm between these modes corresponds to the MO resonator length and indicates a disturbance of the MO by optical feedback from the PA.

As expected, the observed feedback related effects are significantly reduced for the MOPA with a 30% AR coated MO. Here, extended operating ranges with stable dual-wavelength single mode emission enable a flexible choice of output powers for the application without requiring spectral recalibrations of the Raman spectrometer.

Implementing an optical isolator completely suppresses optical feedback and dual-wavelength single mode emission is obtained along the entire power range. Without amplification, the plot shows peak emission wavelengths correponding to the MO spectra in figure 6. With amplifier operation, a potential heat transfer from the PA to the MO for this device shifts both emission wavelengths by about 60 pm (<1 cm^{-1}) along the observed power range.

Based on the obtained electro-optical and spectral characteristics in CW operation, the MOPA in concept 2 is selected for further investigations.

Figure 10 shows the corresponding normalized lateral intensity distributions of the near field, beam waist and far field at 1 W of output power. They are measured according to the method of the moving slit (ISO Standard 11146).

Near field widths of about 210 μm ($1/e^2$) fit to the aperture width expected for the 2 mm long, 6° tapered section. Deviations in the profile shapes might result from different optical coupling at both wavelengths, caused by previously reported spatial asymmetries of 785 nm Y-branch DBR laser emissions at higher injection currents [9]. Both beam waist profiles show distinct 4 μm wide central lobes ($1/e^2$) with a power content of $P_{CL} \approx 90\%$ and a varying number of lateral side lobes. Far field angles of about 18° ($1/e^2$) result in beam propagation ratios of $M^2 = 1.2$ ($1/e^2$). In contrast to free-running Y-branch DBR diode lasers, the positions of the far field intensity distributions at both wavelengths overlap and therefore enable easy beam shaping and fiber coupling.

The measured astigmatism, i.e., the power-dependent longitudinal distance of the beam waist with respect to the front facet of the laser, is about 0.6 mm. It changes by 25 μm W^{-1}. Fiber coupling simulations for 25 μm multimode fibers with a numerical aperture of NA = 0.2 showed that increasing the astigmatism by 75 μm, corresponding to a 3 W power increase, only showed a 3% reduction of the obtained coupling efficiency. The flexibility in selecting excitation powers provided through the MOPA concept should therefore also be fully available for applications with fiber-based experimental setups and probes.

In order to demonstrate the performance outside of the above comparison, figure 11 shows the power-voltage-current of the concept 2 MOPA for injection currents up to $I_{TA} = 3$ A, respectively. The MOPA provides maximum optical output powers of 2.7 W (λ_1) and 2.6 W (λ_2) at corresponding electro-optical efficiencies of 48% (λ_1) and 46% (λ_2). Considering all applied injection currents, a power consumption of 6.6 W is measured and results in an overall electro-optical efficiency of about 40%. The spectral characteristics in figure 12 confirm

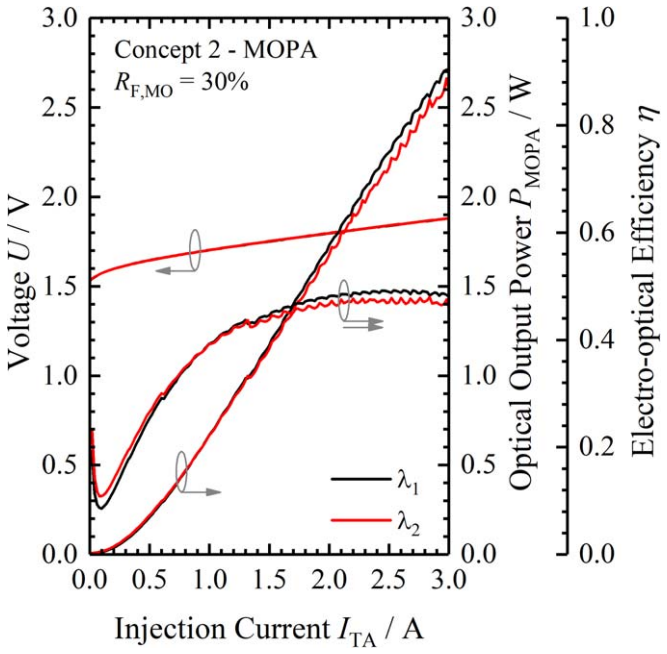

Figure 11. Power-voltage-current characteristics for the concept 2 MOPA at 50 mW pump power.

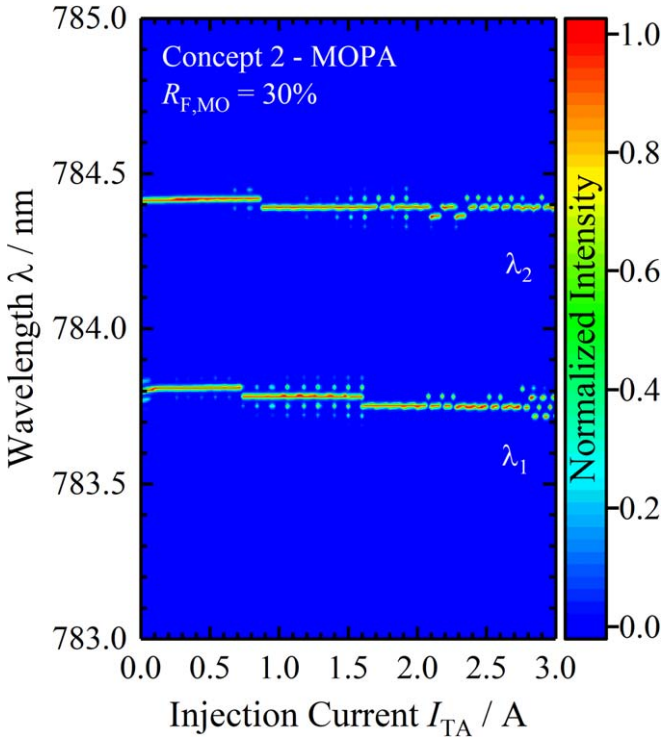

Figure 12. Spectral characteristics for the concept 2 MOPA at 50 mW pump power.

the above discussed observations and reveal laser emission wavelengths within spectral windows <0.15 nm (3 cm^{-1}) along the entire power range.

6. Summary

785 nm dual-wavelength MOPAs with a footprint of 5 mm × 25 mm have been presented and experimentally compared up to 1 W of output power. All light sources provided narrowband laser emissions with spectral

distances of 0.6 nm (10 cm^{-1}) and individual spectral widths <20 pm (FWHM). The MOPAs based on Y-branch diode lasers and AR coated tapered amplifiers showed different extents of feedback related mode hops and simultaneous longitudinal modes along the power range. At all settings, measured longitudinal modes remained within spectral windows <0.15 nm (3 cm^{-1}), suitable for applications such as Raman spectroscopy and shifted excitation Raman difference spectroscopy. In comparison, a higher front facet reflectivity of 30% significantly reduced these feedback related effects and enabled extended operating ranges with dual-wavelength single mode laser emissions. Integrating a miniaturized 30 dB optical isolator helped to eliminate the observed behavior. Lateral beam propagation ratios of 1.2 ($1/e^2$) allow for easy beam shaping and fiber coupling. Outside of the experimental comparison, the developed MOPAs provide up to 2.7 W of optical output power available for applications. For future devices, adapting the packaging for implementation of optical isolators will help to provide mode-hop free CW power scaling towards multiple Watts.

Acknowledgments

The authors acknowledge the support from Alexander Sahm and Arnim Ginolas for the packaging of the laser diodes and all colleagues involved in this study.

Data availability statement

The data that support the findings of this study are available upon reasonable request from the authors.

Funding

This work was partially supported by the Federal Ministry of Education and Research (BMBF) by means of the project I4S (grant numbers 031A564C, 031B513C, 031B1069C) and the 'Forschungsfabrik Mikroelektronik Deutschland (FMD)' framework under ref. 16FMD02.

ORCID iDs

André Müller https://orcid.org/0000-0001-8496-3004

References

[1] McCreery R L 2000 *Raman Spectroscopy for Chemical Analysis* (New York: Wiley-Interscience)
[2] Demtröder W 1981 *Laser Spectroscopy - Basic Concepts and Instrumentation* (Berlin: Springer)
[3] Van Duyne R P, Jeanmaire D L and Shriver D F 1974 Mode-locked laser Raman spectroscopy. A new technique for the rejection of interfering background luminescence signals *Anal. Chem.* **46** 213
[4] Kögler M and Heilala B 2020 Time-gated Raman spectroscopy—a review *Meas. Sci. Technol.* **32** 012002
[5] Asher S A and Johnson C R 1984 Raman spectroscopy of a coal liquid shows that fluorescence interference is minimized with ultraviolet excitation *Science* **225** 311
[6] Asher S A 2002 *Ultraviolet Raman Spectrometry in Handbook of Vibrational Spectroscopy* (Chichester: Wiley)
[7] Wei D, Chen S and Liu Q 2015 Review of fluorescence suppression techniques in raman spectroscopy *Appl. Spectrosc. Rev.* **50** 387
[8] McCain S T, Willett R M and Brady D J 2008 Multi-excitation Raman spectroscopy technique for fluorescence rejection *Opt. Express* **16** 10975
[9] Lister A P, Highmore C J, Hanrahan N, Read J, Munro A P S, Tan S, Allan R N, Faust S N, Webb J S and Mahajan S 2022 Multi-Excitation raman spectroscopy for label-free, strain-level characterization of bacterial pathogens in artificial sputum media *Anal. Chem.* **94** 669–77
[10] De Luca A C, Dholakia K and Mazilu M 2015 Modulated Raman spectroscopy for enhanced cancer diagnosis at the cellular level *Sensors* **15** 13680–704
[11] Woolford L, Chen M, Dholakia K and Herrington C S 2018 Towards automated cancer screening: Label-free classification of fixed cell samples using wavelength modulated Raman spectroscopy *J. Biophotonics* **11** e201700244
[12] Cooper J B, Abdelkader M and Wise K L 2013 Sequentially shifted excitation raman spectroscopy: novel algorithm and instrumentation for fluorescence-free raman spectroscopy in spectral space *Appl. Spectrosc.* **67** 973
[13] Cooper J B, Marshall S, Jones R, Abdelkader M and Wise K L 2014 Spatially compressed dual-wavelength excitation Raman spectrometer *Appl. Opt.* **53** 3333
[14] Conti C, Botteon A, Bertasa M, Colombo C, Realini M and Sali D 2016 Portable sequentially shifted excitation raman spectroscopy as an innovative tool for *in situ* chemical interrogation of painted surfaces *Analyst* **141** 4599–607
[15] Shreve A P, Cherepy N J and Mathies R A 1992 Effective rejection of fluorescence interference in Raman spectroscopy using shifted excitation difference technique *Appl. Spectrosc.* **46** 707
[16] Sumpf B, Maiwald M, Müller A, Fricke J, Ressel P, Bugge F, Erbert G and Tränkle G 2015 Comparison of two concepts for dual-wavelength DBR ridge waveguide diode lasers at 785 nm suitable for shifted excitation Raman difference spectroscopy *Appl. Phys. B* **120** 261

[17] Maiwald M, Müller A, Sumpf B and Tränkle G 2016 A portable shifted excitation Raman difference spectroscopy system: device and field demonstration *J. Raman Spectrosc.* **47** 1180
[18] Dwivedi Y 2020 *Concept and Applications of standoff Raman spectroscopy techniques in Molecular and Laser Spectroscopy Advances and Applications* 2 (Amsterdam: Elsevier)
[19] Agrawal G V and Dutta N K 1993 *Semiconductor Lasers* IInd edn (New York: Van Nostrand Reinhold)
[20] Müller A, Maiwald M and Sumpf B 2019 Compact diode laser-based dual-wavelength master oscillator power amplifier at 785 nm *IEEE Photon. Technol. Lett.* **31** 1120
[21] Sumpf B, Theurer L S, Maiwald M, Müller A, Maaßdorf A, Fricke J, Ressel P and Tränkle G 2021 783 nm wavelength stabilized DBR tapered diode lasers with a 7 W output power *Appl. Opt.* **60** 5418
[22] Tkach R and Chraplyvy A 1986 Regimes of feedback effects in 1.5 μm distributed feedback lasers *J. Lightwave Technol.* **4** 1655
[23] Christensen M, Christensen M, Zink C, Jamal M T, Hansen A K, Jensen O B and Sumpf B 2021 Measuring the sensitivity to optical feedback of single-frequency high-power laser diodes *JOSA B* **38** 885
[24] Erbert G, Bugge F, Knauer A, Sebastian J, Thies A, Wenzel H, Weyers M and Tränkle G 1999 High-power tensile-strained GaAsP-AlGaAs quantum-well lasers emitting between 715 and 790 nm *IEEE J. Sel. Top. Quantum Electron.* **5** 780
[25] Ressel P, Erbert G, Zeimer U, Häusler K, Beister G, Sumpf B, Klehr A and Tränkle G 2005 Novel passivation process for the mirror facets of high-power semiconductor diode lasers *IEEE Photonic. Technol. Lett.* **17** 962
[26] Pittroff W *et al* 2001 Mounting of high power laser diodes on boron nitride heat sinks using an optimized Au/Sn metallurgy *IEEE Trans. Adv. Packag.* **24** 434